1 **Barrier breaching versus overwash deposition: parameterizing the morphologic impact of**

2 **storms on coastal barriers**

3 Jaap H. Nienhuis*, Leoni G.H. Heijkers, Gerben Ruessink

4 Department of physical geography, Utrecht University, Utrecht, NL

5 *Corresponding author address: VMA 4.88, Princetonlaan 8a, Utrecht, NL, j.h.nienhuis@uu.nl

6 **Key points**

7   1. New predictor for barrier island breaching and washover deposition

8   2. Idealized Delft3D morphodynamic simulations of barrier island overwashing flows,

9   washover formation, and inlet formation

10   3. Tests of new predictor against Delft3D simulations and Hurricane Sandy observations

11   shows reasonable correspondence for natural barriers

12 **Abstract**

13   Waves and water level setup during storms can create overwashing flows across barrier

14 islands. Overwashing flows can cause erosion and barrier island breaching, but its sediments can

15 also be deposited as washover fans. These widely different outcomes remain difficult to predict.

16 Here we suggest that breaches develop when the sediment transported by overwashing flows

17 exceed the barrier subaerial volume. We form a simple analytical theory that estimates

18 overwashing flows from storm characteristics, barrier morphology, and dune vegetation, and can

19 be used to assess washover deposition and breaching likelihood. Barrier width and storm surge

20 height appear as two important controls on barrier breaching. We test our theory with the

21 hydrodynamic and morphodynamic model Delft3D as well as with field observations of 21

22 washover fans and 6 breaches that formed during hurricane Sandy. There is reasonable

23 correspondence for natural but not for developed barrier coasts. Our analytical formulations for

24 breach formation and overwash deposition can be used to improve long-term barrier island

25 models.

1 Introduction

26

27   Storms can have large impacts on barrier islands. Overwashing flows and waves can
28 move sediment across barrier islands and result in washover deposition (Fig. 1a) or barrier island
29 breaching (Fig. 1b) (Pierce, 1970). These outcomes are strongly sensitive to barrier
30 characteristics and storm intensity (Suter et al., 1982; Plomaritis et al., 2018). Hurricane Sandy
31 hit the U.S. East Coast in 2012 and resulted in widespread overwashing and numerous breaches
32 (Fig. 1) (Sopkin et al., 2014). Breaching is likely to be increasingly common as a result of sea-
33 level rise (Passeri et al., 2020). At the same time, washover deposition is a critical landward-
34 directed sediment flux that can support barrier aggradation and prevent barrier drowning.
35 Reliable predictions of barrier breaching and washover deposition prior to landfall remain
36 difficult.

37   In this study we propose that barrier islands breach when the cumulative sediment flux of
38 an overwashing flow exceeds the barrier subaerial volume. A washover deposit forms when an
39 overwashing flow does not erode the barrier down to sea-level. Washover volumes increase as
40 overwashing flows approach the washover-to-breaching threshold.

41   The objective of this study is to test this theory using Delft3D simulations and
42 observations from hurricane Sandy. We systematically explore the effect of barrier island
43 morphology, storm characteristics, and dune vegetation on overwashing flows and the
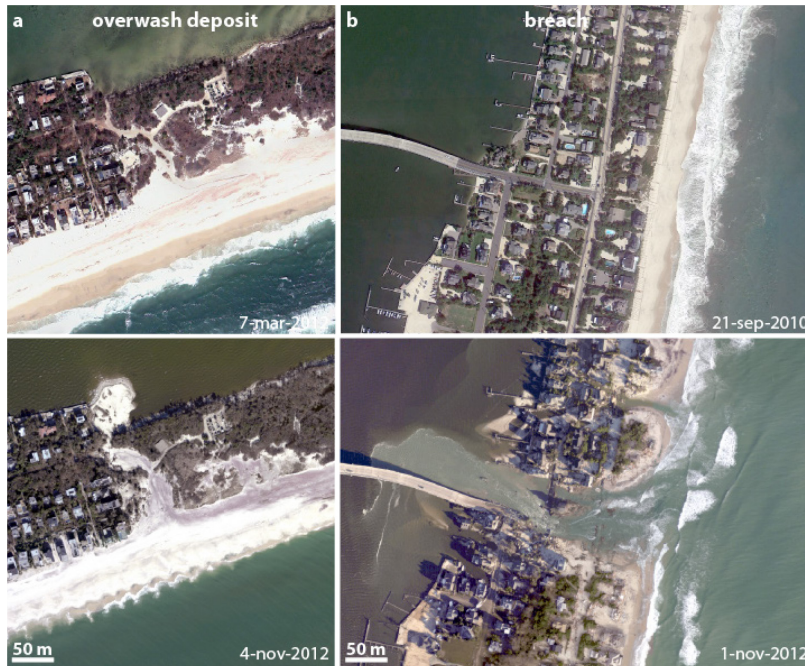44 morphologic response of barrier coasts.

Figure 1. Storm response to Hurricane Sandy, showing (**a**) the deposition of a washover fan and (**b**) the formation of a breach. These examples are #24 and #1, respectively, of the supplementary data table.

2   Background

2.1   Overwashing flows

Storm winds setup surges and generate waves that can lead to erosion of beaches and dunes. These impacts are often assessed based on relative elevation of wave runup and water levels against the dune toe or dune crest (Sallenger, 2000). Waves and water levels reaching the dune toe can induce slumping and dune erosion. Overwashing flows occur when wave runup and/or water levels exceed the island elevation (Fisher & Stauble, 1977; Kobayashi, 2010).

Overwashing flows and sediment transport have been studied in the laboratory and in the field (Donnelly et al., 2006). They are highly variable over time and space and can flow in both directions across barrier islands (Wesselman et al., 2018; Goff et al., 2019) depending on storm characteristics and the phase lag of lagoon water levels compared to the ocean (Shin, 1996).

Several studies have aimed to determine the relative influence of wind, waves, infragravity waves, and water level gradients on water and sediment fluxes transported in overwashing flows. A recent study by Engelstad et al (2018) on an overwashing flow across the

3

63   Dutch island of Schiermonnikoog showed that sediment transport was primarily controlled by

64   currents, but that occasional high sediment concentrations were found on wave infragravity

65   timescales. Wave conditions (McCall et al., 2010) and foredune size (de Winter et al., 2015) are

66   important controls on foredune erosion and determining locations of overwashing flows, whereas

67   the water level gradient controlled the amount of overwashing sediment and its deposition in the

68   back barrier.

69   The evolution and magnitude of overwashing flows also depends on dune morphology

70   and vegetation patterns (Houser et al., 2008; Kobayashi, 2010; Passeri et al., 2018), which can

71   constrict the flow and deepen the throat. Flow acceleration through the throat can also widen the

72   gap (Houser et al., 2008).

73   Predictions for sediment fluxes during wave overwashing in the absence of currents have

74   been formulated using laboratory studies (Williams, 1978; Nguyen et al., 2009). These formulae

75   show reasonable correspondence to a variety of field settings and highlight a quadratic

76   dependence of wave overwash fluxes to wave runup. A similar wave overwash model from

77   Kobayashi et al (2010) show the sensitivity of the initial barrier geometry on barrier resilience to

78   overwash. Their results are validated by experimental and field evidence but do not include the

79   effect of currents on sediment fluxes. We refer to Donnelly (2006) for a review on overwashing

80   flows.

81   *2.2   Washover deposition*

82   Washovers form through the settling of sediment transported by overwashing flows

83   (Woodruff et al., 2008). A compilation from Hudock et al (2014) shows large variability in

84   washover area, but many are less than 1 km^2. Carruthers et al (2013) report washover volumes

85   normalized per unit width alongshore and obtain a median of 30 m^3/m. A scaling analysis of

86   experimental and natural washover deposits finds that they are typically longer than they are

87   wide, with a width/length ratio of ~0.5 (Lazarus, 2016).

88   The length and size of washover deposits is controlled by storm characteristics (Morton

89   et al., 2003). Barrier islands formed by washover fans could therefore reflect long-term storm

90   history, and island width could be limited by the maximum transport distance of storm into the

91   lagoon (Hayes, 1979; Leatherman, 1979). Barrier island land cover such as the type of

92   development or vegetation can also affect washover characteristics (Sedrati et al., 2011; Rogers

93   et al., 2015), as does competition for flow from neighbouring washover throats (Lazarus &

94   Armstrong, 2015). The latter can result in a characteristic spacing of washover deposits.

95   *2.3   Breaching*

96   Overwashing flows can also lead to barrier island breaching. Many studies of barrier

97   breaching focus on the exposed U.S. East Coast, where storm surges from hurricanes and

98   extratropical storms frequently result in breaches (Kraus & Hayashi, 2005). Ground-penetrating

99   radar images of the North Carolina outer banks shows that at least 24% of the modern barrier

100 island chain has been breached (Mallinson et al., 2010). Breaching also occurs along barrier

101 coasts elsewhere, including the Ebro Delta, California, and Santa Rosa Island (Sánchez-Arcilla

102 & Jiménez, 1994; Kraus et al., 2002; Morgan, 2009).

103   Models generated from breaches of sand dikes (Visser, 2001; Tuan et al., 2008) focus on

104 the expansion of the overwashing throat and find that breaches originate by head cutting and

105 erosion along the dune-side of the throat. Basco and Shin (1999) found that surge level

106 differences between ocean and bay regulate flow conditions and are an important predictor of

107 barrier island breaching. Further evidence from model and field studies specifically showed that

108 the timing of surge levels between the ocean and the bay, and the resulting water level gradients,

109 affect breaching likelihood and direction (Smallegan et al., 2016). A large time lag in surge

110 levels between the ocean and the bay make breaching towards the ocean more likely (Shin,

111 1996).

112   Site-specific process-based models of dune erosion and barrier breaching include Delft3D

113 (Deltares, 2014) and XBeach (Roelvink et al., 2009; Van Dongeren et al., 2009; McCall et al.,

114 2010; Elsayed & Oumeraci, 2016). De Vet et al (2015) applied XBeach on the well-documented

115 "Wilderness" breach on Fire Island, NY and find that bed roughness, including vegetation

116 roughness, is a sensitive and poorly constrained parameter that is important for properly

117 hindcasting the emergence of a breach. Recent model-coupling between Delft3D and XBeach

118 (e.g., van Ormondt et al., 2020) show promise for forecasting barrier breaching, but accurate,

119 site-specific process-based simulations of overwashing flows and barrier breaches remain

120 challenging.

121   On a conceptual level, Kraus et al (2002) postulated that breach susceptibility is

122   controlled by the storm surge water level and is inversely proportional to the tidal range, used as

123   a proxy for barrier island elevation. A modelling study by Nienhuis and Lorenzo-Trueba (2019a)

124   also showed that breaches are more common in micro-tidal settings, in their case because it

125   limits the lifetime of existing tidal inlets and increases potential tidal prism available to new

126   breaches. Their model also suggests that, similar to alongshore competition for washover flow

127   (Lazarus & Armstrong, 2015), there is alongshore competition for tidal flow that results in a

128   characteristic spacing of successful breaches. However, there remains a large gap in model

129   studies between detailed, site-specific simulations of overwashing flows, and large-scale barrier

130   island models.

131   Here we try to bridge the gap between process-based site-specific models vs. conceptual

132   studies of breaching and washover deposition. We develop an analytical theory of overwashing

133   flows that can aid short-term risk assessment and help parameterize storm impact for long-term

134   morphologic models. We test this theory using an idealized Delft3D model of overwashing flows

135   on storm timescales combined with observations of washovers and breaches from Hurricane

136   Sandy.

137   **3   Analytical theory**

138   In our theoretical model we define the washover volume as the total overwashing

139   sediment flux into the lagoon, bayward of original barrier shoreline. Following Shin (1996), we

140   classify a barrier as breached when the dune gap erosion exceeds mean sea-level and there is no

141   subaerial barrier left after the storm. Here, we hypothesize that barriers breach when the storm-

142   integrated overwashing flux V_{ow} (m^3) exceeds the barrier subaerial volume V_{bar} (m^3) (Fig. 2).
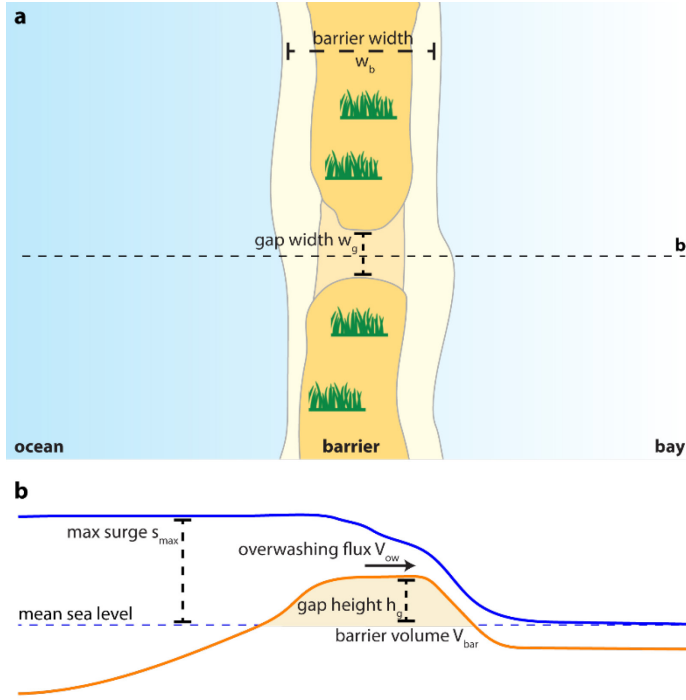
143

Figure 2: Conceptual model of an overwashing flow through a dune gap. (a) Plan-view
barrier coast separating the bay from the ocean, **(b)** cross-section through the dune gap
highlighting the overwashing flux V_{ow} and the barrier volume V_{bar}.

We use a simple sediment transport-based predictor to relate storm conditions to the
overwashing sediment flux and dune gap erosion. This predictor is based on steady, uniform
flow for bed shear stress (e.g. depth-slope product) and Engelund and Hansen (1967) for the
resulting sediment transport. We do not simulate (wave-dominated) erosion and/or formation of
a dune gap, but instead follow earlier studies that showed that water level gradients are a first-
order control on overwashing flows, washover deposition, and barrier breaching (Basco & Shin,
1999; McCall et al., 2010; Engelstad et al., 2018). Combining the depth-slope product (ρghS)
and Engelund and Hansen (1967) yields the following prediction for overwashing sediment
transport through the dune gap $Q_{ow,t}$ (m^{3}s^{-1}),

$$Q_{ow,t}(t) = \frac{0.05}{C_f}\left(\frac{\rho ghS}{(\rho_s-\rho)\cdot g\cdot D_{50}}\right)^{2.5} D_{50}\cdot\sqrt{R\cdot g\cdot D_{50}}\cdot w_g, \quad (1)$$

where C_f is a non-dimension friction factor, ρ is the density of water (~1000 kg m^{-3}), ρ_s is the
density of sand (~2650 kg m^{-3}), h is the water depth (m), S is the water surface slope (m m^{-1}), g is

7

159   gravity (m s^{-2}), D_{50} is the median grain size (m), R is the relative density of sand (~1.65), w_g is

160   the dune gap width (m).

161   We estimate the water depth h midway through the gap as $\frac{1}{2}(s_{max} - h_g)$, where s_{max} is

162   the maximum surge level (m) and h_g is the height of the dune gap (m) (Fig. 2b). For simplicity,

163   we assume the bay water level is zero (mean sea level). The water surface slope can then be

164   approximated as the surge level $s(t)$ (m) as a function of time t (s), divided by the barrier width

165   w_b (m).

166   Combined, we can simplify equation (1) to,

167     $$Q_{ow,t}(t) = \frac{0.05}{C_f}\left(\frac{s_{max}-h_g}{2}\right)^{2.5}\left(\frac{s(t)}{w_b}\right)^{2.5}\frac{\sqrt{g}}{R^2 D_{50}} \cdot w_g, \tag{2}$$

168   and write a predictive equation for the integrated eroded sediment volume of the barrier $V_{ow,t}$

169   (m^3),

170     $$V_{ow,t} = \int_0^{T_{storm}} Q_{ow,t}(t) \cdot c_c \, dt, \tag{3}$$

171   where T_{storm} (s) is the duration of the storm. c_c is a calibration coefficient of 0.1 to reduce the

172   observed overprediction of our theory compared to the Delft3D simulations, $V_{ow,d3d}$. We found

173   (in section 5.3) that an unadjusted predictor (without c_c) resulted in an overprediction of the

174   sediment flux of about a factor ~10. This is likely caused by the linearity of our predictor,

175   including the assumption of a constant water depth h, and the absence of a threshold for motion.

176   For a triangular surge timeseries $s(t) = s_{max} \cdot \left(1 - \left|\frac{2t}{T_{storm}} - 1\right|\right)$, of which the integral

177   is identical to $s(t) = s_{max}\frac{t}{T_{storm}}$, $V_{ow,t}$ evaluates to,

178     $$V_{ow,t} = \frac{\sqrt{2}}{560}\frac{T_{storm}\sqrt{g}}{D_{50}R^2 C_f}(s_{max} - h)^{2.5}\left(\frac{s_{max}}{w_b}\right)^{2.5}c_c \cdot w_g. \tag{4}$$

179   We expect the barrier to breach if $V_{ow,t}$ exceeds the subaerial barrier volume V_{bar}, where

180     $V_{bar} = \frac{1}{2}h_g \cdot w_b \cdot w_g$. The factor $\frac{1}{2}$ is included because the barrier profile underneath the dune gap

181   is roughly triangular towards the beach and the lagoon (Fig. 2b). We write the theoretical

182   normalized overwash volume $V_{norm,t}$ as,

8

$$V_{norm,t} = \frac{V_{ow,t}}{V_{bar}} = \frac{c_c \cdot w_g \cdot \frac{\sqrt{2}}{560} \cdot \frac{T_{storm}\sqrt{g}}{D_{50}R^2 C_f}(s_{max}-h_g)^{2.5}\left(\frac{s_{max}}{w_b}\right)^{2.5}}{\frac{1}{2}h_g \cdot w_b \cdot w_g}, \tag{5}$$

where a barrier is expected to breach if $V_{norm,t} > 1$. We expect the subaerial barrier to be maintained if $V_{norm,t} < 1$. If that is the case and the overwashing sediment flux will deposit as a washover fan, $V_{ow,t}$ will give an indication of the washover fan volume.

Equation (5) estimates that the overwash volume scales with surge height to the power 5 because it affects the depth of the overwashing flow as well as the water surface slope. Breaching probability scales with barrier width to the power -3.5. It predicts that overwash volumes scale linearly with dune gap width, and that dune gap width does not affect breaching probabilities. It is relatively straightforward to evaluate and apply in data-poor environments. Although not applied here, it can be adapted to account for varying water levels in the lagoon as well, including surges that lead to flow towards the ocean.

Some of the trends in equation (5) align with observations from Wesselman et al. (2019), who found that dune height compared to surge elevation is important for sediment fluxes through dune gaps. Gap width was found to be less important and mostly linearly related to sediment fluxes except for smaller widths where flow contraction became significant. The prediction here (eq. 1-5) does not account for the effect of flow contraction nor the potential effect of neighboring overwashes that lower water level gradients. It also neglects many other important processes that occur in overwashing flows such as sheet-flow transport (Basco & Shin, 1999; Tuan et al., 2008).

We will test our theoretical predictions against Delft3D model simulations and observations from hurricane Sandy for varying storm conditions (T, s_{max}) and barrier morphologies (w_b, h_g) and barrier land cover (C_f). These data sources provide modelled and observed washover volumes ($V_{ow,d3d}$ and $V_{ow,obs}$) that we can compare against the predicted washover volume ($V_{ow,t}$). We will also test if breaches occur for $V_{norm,t} > 1$ by comparing it to $V_{norm,d3d} = \frac{V_{ow,d3d}}{V_{bar}}$ and $V_{norm,obs} = \frac{V_{ow,obs}}{V_{bar}}$.

4   Methods

Section 4.1 describes the Delft3D model setup and section 4.2 describes the Hurricane Sandy analyses.

211 *4.1   Delft3D model setup*

212   We simulate the morphodynamics of overwashing flows using the hydro- and

213 morphodynamic model Delft3D (Deltares, 2014). Delft3D couples shallow water equations with

214 sediment transport formulas to simulate morphologic change. We use idealized barrier island

215 geometries and simulate overwashing flows through a dune gap. Storm surge levels and

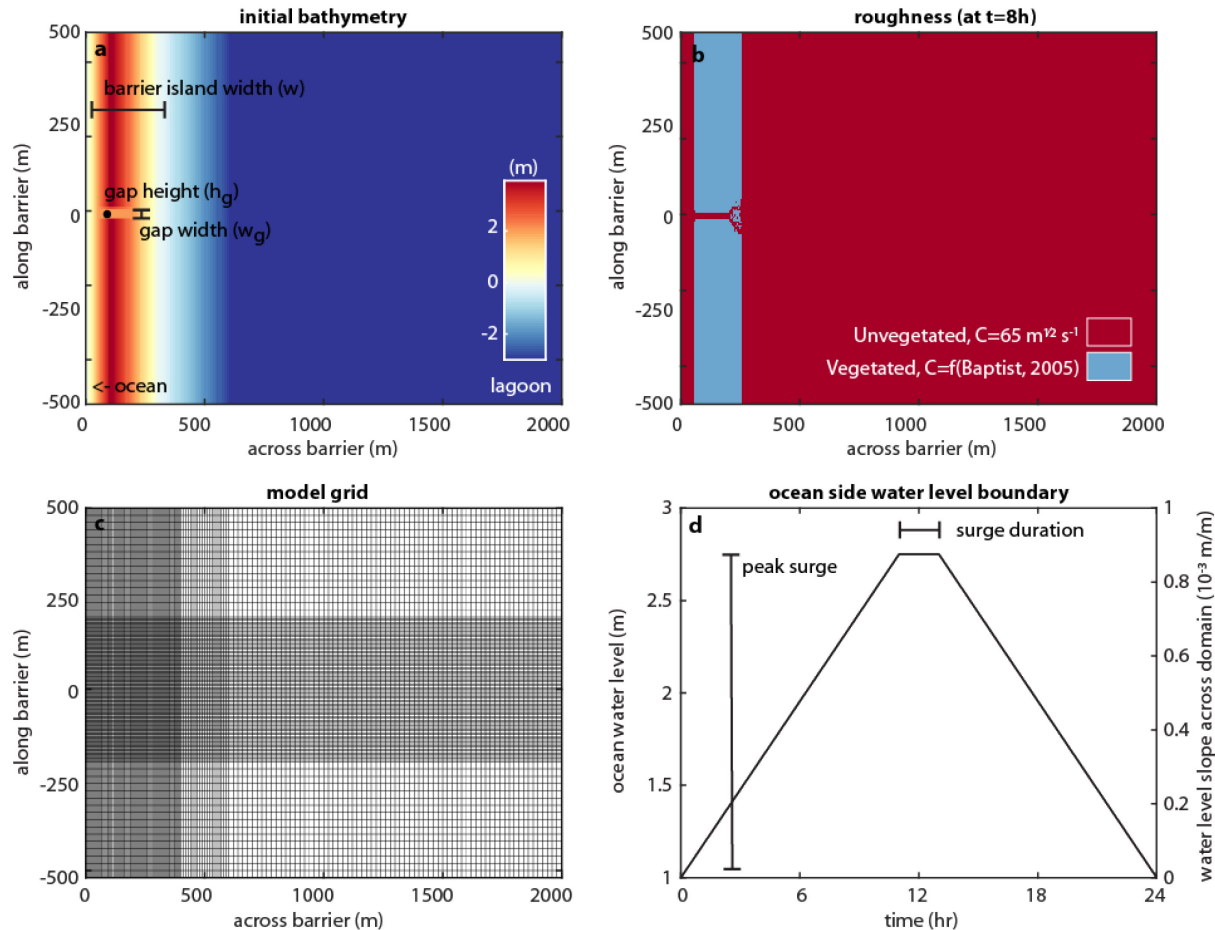216 durations are represented as a water level boundary on the ocean side of the domain (Fig. 3).

218 **Figure 3: Delft3D model domain and setup to study washover deposition and barrier**

219 **breaching. (a)** Initial bathymetry and barrier morphological parameters, (**b**) bed roughness (after

220 8 hours of flow to illustrate the model dynamic effects of overwashing flow), (**c**) model grid, and

221 (**d**) model boundary conditions across the domain. Model setup files and model output is

222 available at dx.doi.org/10.17605/OSF.IO/3KNXA.

223   We vary barrier morphology and storm characteristics between 139 model simulations

224   (Fig. 3, Table 1). The model setup is similar to one used in an earlier study by Nienhuis et al

225   (2018), who investigated the morphologic evolution of river levee gap into avulsions and

226   crevasse splays. A notable difference here is that there is no sediment supply from the ocean

227   boundary. As opposed to river crevasses, dune gaps cannot heal but instead simply stop

228   expanding when the storm recedes.

229   The initial bathymetry of the domain consists of a 1 km long coastal barrier and an

230   adjacent lagoon. Barrier widths vary between 150 and 400 m, with the rest of the 2 km cross-

231   profile modelled as a 3 m deep lagoon (Fig. 3). The domain consists of 172 by 112 cells in the

232   cross-shore and alongshore direction, respectively. The resolution ranges from 5 by 5 m near the

233   dune gap to 20 by 20 m along the sides and into the lagoon. The dune gap is in the middle of the

234   simulated barrier island. We vary the height and width of the gap between simulations (Table 1)

235   and use a uniform 0.2 mm sand across the barrier and lagoon.

236   The effect of vegetation is included using the Baptist (2009) 'Trachytope' function,

237   which estimates an effective bed roughness depending on the vegetation height and density

238   relative to the water depth (Deltares, 2014). We use values typical for American Beachgrass.

239   Vegetation height is 0.5 m, stem density is 50 m^{-2}, and the aerial fraction is between 0% and 20%

240   for different model runs (Biel et al., 2017). Note that these simulations are not aimed at

241   representing any specific barrier island. Although the observations are limited to Hurricane

242   Sandy, the spread between model scenarios is meant to encompass storm characteristics and

243   barrier island morphologies globally.

244   The water level boundary condition on the ocean side of the barrier is prescribed as a

245   simplified storm surge lasting 24 hours (Fig. 3d). We vary the peak surge water level and the

246   duration of the peak between simulation to represent different storm magnitudes. Note that we

247   use a slightly altered surge time series then what is assumed in eq. 4. We therefore use eq. 3 to

248   obtain $V_{ow,t}$. The water level at the lagoon is kept constant at 1 m, such that there is no return

249   flow possible through the dune gap. Breaches and washover fans can only appear on the lagoon

250   side of the barrier. There is no flow possible through the side boundaries up and down coast from

251   the breach.

252   As the water level rises on the ocean side, the dune gap becomes wet and a water surface

253   slope appears across the island. Sediment transport fluxes are calculated following van Rijn

254   (2007), using a 0.1 m water depth threshold for sediment transport for model stability. This is a

255   different sediment transport predictor than what we use in our theoretical model (eq. 1). We

256   choose van Rijn (2007) for our Delft3D simulation because it is more accurate than Engelund

257   and Hansen (1967). We use the latter for our theoretical model because it does not require many

258   parameters that could be difficult to assess in the field. Dry cells along the edges of the dune gap

259   erode if erosion occurs in the dune gap itself. Delft3D uses a "dry cell erosion factor", set here to

260   0.9, to distribute the erosion between the wet cell and the dry cell. This factor can be viewed as a

261   simple proxy for a critical bed slope for bank failure.

262   Overwashing flows are generated from a water level gradient across the barrier island

263   through the dune gap. Based on this gradient, the barrier width and roughness, and available

264   subaerial barrier volume, morphologic simulations then form either washover deposits or result

265   in barrier breaching. See Table 1 for an overview of model settings. The supplementary data for

266   the model code and model output to reproduce our findings are available at

267   dx.doi.org/10.17605/OSF.IO/3KNXA.

268   **Table 1.** Delft3D model simulation settings

Parameter	Value	Units	Description
s_{max}	2…4	m	peak surge above MSL
T	0…10	h	surge duration, different from T_{storm}
w	150…400	m	barrier width
h_g	1...2.5	m	gap height above MSL
w_g	10…100	m	gap width
ocean	f(s,T)	m	function of storm surge and duration, see Fig. 3d
lagoon	1	m	lagoon water level boundary
frac. 1	0…0.2		fraction of the island using Trachytope 153 (Baptist 1)
frac. 2	1…0.8		fraction of the island using Trachytope 105 (Bedforms quadratic)
hv	0.5	m	vegetation height
n	50	m^{-1}	stem density
Cd	1		drag coefficient of vegetation
Cb	65	$m^{0.5} s^{-1}$	bed roughness chezy
C_f	$3.3 \cdot 10^{-3}$ ... $4.2 \cdot 10^{-3}$		flow roughness (including vegetation, for ~ 0.5 m water depth)
Dryflc	0.1	m	Threshold depth for drying and flooding
EqmBc	FALSE		Equilibrium sand concentration profile at inflow boundaries

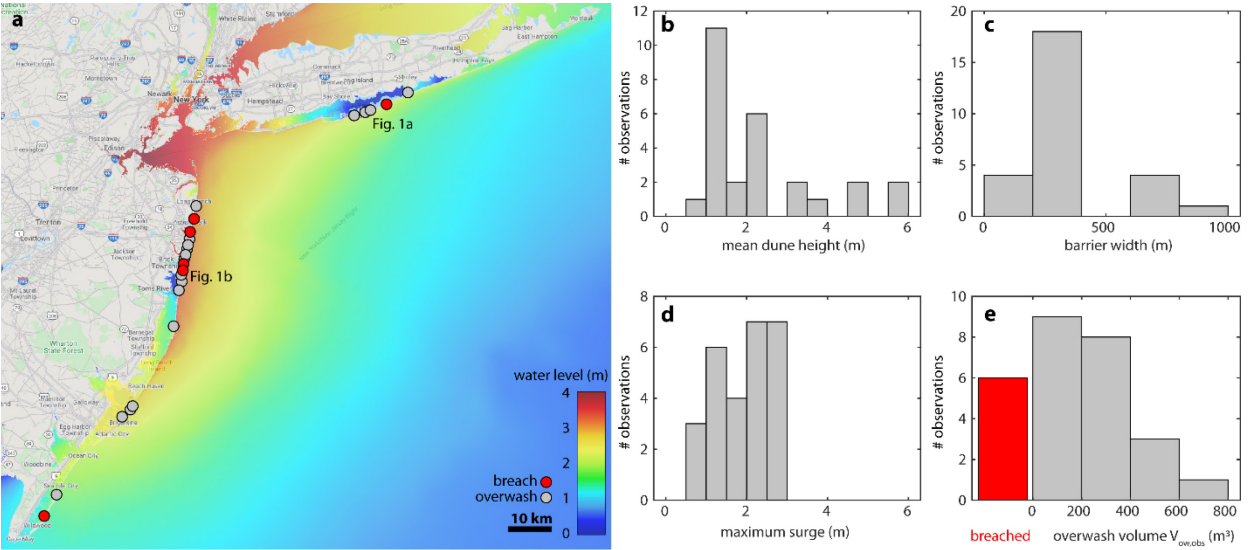|			
SedThr	0.1	m	Minimum water depth for sediment computations
ThetSD	0.9		Factor for erosion of adjacent dry cells
RhoSol	2650	kg m^{-3}	Specific density
d_{50}	0.0002	m	Median sediment diameter
CdryB	1600	kg m^{-3}	Dry bed density

269

4.2 *Hurricane Sandy analyses*

Figure 4. (a) Locations of washovers (grey) and breaches (red) overlain on the maximum water levels during hurricane Sandy. **(b-e)** distributions of storm barrier characteristics of the 27 locations.

Hurricane Sandy observations allow us to test our theoretical model and our morphodynamic Delft3D simulations. Sandy made landfall on the New Jersey coast on October 29, 2012, and resulted in numerous breaches and washover fans (Sopkin et al., 2014), including the well-documented "Wilderness" breach on Fire Island (van Ormondt et al., 2020). We analyzed 27 overwashing sites, of which 6 resulted in breaches and 21 in overwash fans. For these sites we also retrieved the local storm conditions that led to their formation (Fig. 4).

Storm characteristics are determined using the ADCIRC+SWAN hindcast model simulation (Dietrich et al., 2012) via the Coastal Emergency Risk Assessment (CERA), available at www.coastalrisk.live. ADCIRC is a hydrodynamic model that computes time dependent tide, wind, and pressure driven surge (Luettich et al., 1992). Coupling with SWAN (Booij et al., 1999)

13

285   allows for assessment of wave-driven setup. We use these time-explicit surge hindcasts instead

286   of maximum surge level maps because they allow us to extract water surface slopes. We refer to

287   documentation of CERA for more information.

288   We extract water level timeseries for the lagoon and ocean sides of the barrier islands at

289   the 27 overwashing locations. These timeseries are then converted to surge water level

290   differences across the islands, as well as storm durations. The hindcast simulations for Sandy

291   show that the water level differences between the ocean and lagoon ranged from 0.8 to 2.6 m

292   (Fig. 4d).

293   We use Google Earth images to estimate the pre-storm width and land cover of the

294   overwashing sites. Land cover is categorized as either developed, vegetated, or bare. Chezy

295   roughness coefficients ($= \sqrt{g/C_f}$) of these three land cover types are estimated as 15, 40, and

296   65 $m^{½}$ s^{-1}, respectively, for our theoretical model (Passeri et al., 2018). Dune gap heights are

297   retrieved from the USGS dune crest elevation dataset, which provides maximum and standard

298   deviations of dune elevation of 1km alongshore section (Birchler et al., 2015). We estimate the

299   gap elevation as the maximum dune height minus two standard deviations. Gap widths are

300   assumed to be 100 m.

301   Based on the post-storm NOAA Emergency Response Imagery

302   (https://storms.ngs.noaa.gov/) we characterize each overwashing site as either a breach (e.g., Fig.

303   1a) or a washover deposit (e.g. Fig. 1b). We use these same images to measure the subaerial

304   surface area of each washover deposit. Unfortunately, there is no readily available data to extract

305   washover volumes for the 21 fans in our dataset. We use the washover fan data compiled by

306   Lazarus et al (2016), where field-scale washover volume / area ≈ 0.3 m, to estimate washover

307   volume ($V_{ow,obs}$). For barrier breaches, which do not leave a washover deposit, we set $V_{norm,obs} >$

308   1.

309   **5   Results**

310   *5.1   Mechanics of overwashing flows*

311   We use an example Delft3D simulation of a 300-m wide barrier island to illustrate the

312   model dynamics (Fig. 5). In this case, a breach developed in response to a 3 m storm surge.

313   Water flowing across the gap resulted in high shear stresses, primarily at the back of the dune

314 gap into the lagoon where the water surface slope is greatest. This agrees with model

315 experiments from Visser (2001). Water level gradients in the lagoon are negligible compared to

316 gradients across the barrier, reflecting the relative flow roughness of both environments (Fig.

317 5g).

318   Peak shear stresses of $\sim$ 50 N m^{-2} are observed in the overwashing flows. Critical shear

319 stress for sand movement, $\sim$ 0.15 N m^{-2}, are negligible compared to these peak stresses. High

320 concentrations of sediments are suspended and high gradients of sediment transport cause

321 erosion. Suspended transport magnitude greatly exceeds bedload transport, which is also

322 observed by De Vet (2015) but not in other studies (Shin, 1996). Discrepancies can arise because

323 sheet flow conditions are likely for these (high) Shields numbers, and it is debated whether sheet

324 flow constitutes bed load or suspended load transport.

325   We compared the cumulative sediment transported across the barrier island ($V_{ow,d3d}$) with

326 the subaerial volume of the barrier under the overwashing throat (V_{bar}). The overwashing flow

327 transported approximately $60 \cdot 10^3$ m^3 across the barrier. The subaerial barrier, on average, 1.67 m

328 high, 300 m wide, and the gap extends 50 m alongshore, comprising a volume of $25 \cdot 10^3$ m^3. The

329 result is a normalized barrier overwash $V_{norm,d3d}$ ($V_{ow,d3d} / V_{bar}$) of about $\sim$2.4 at the end of the

330 storm. A breach occurred. The trend of the overwash timeseries shows that the greatest transport

331 occurred after the storm surge peak. Only $\sim$20% of the overwashing flux is transported during
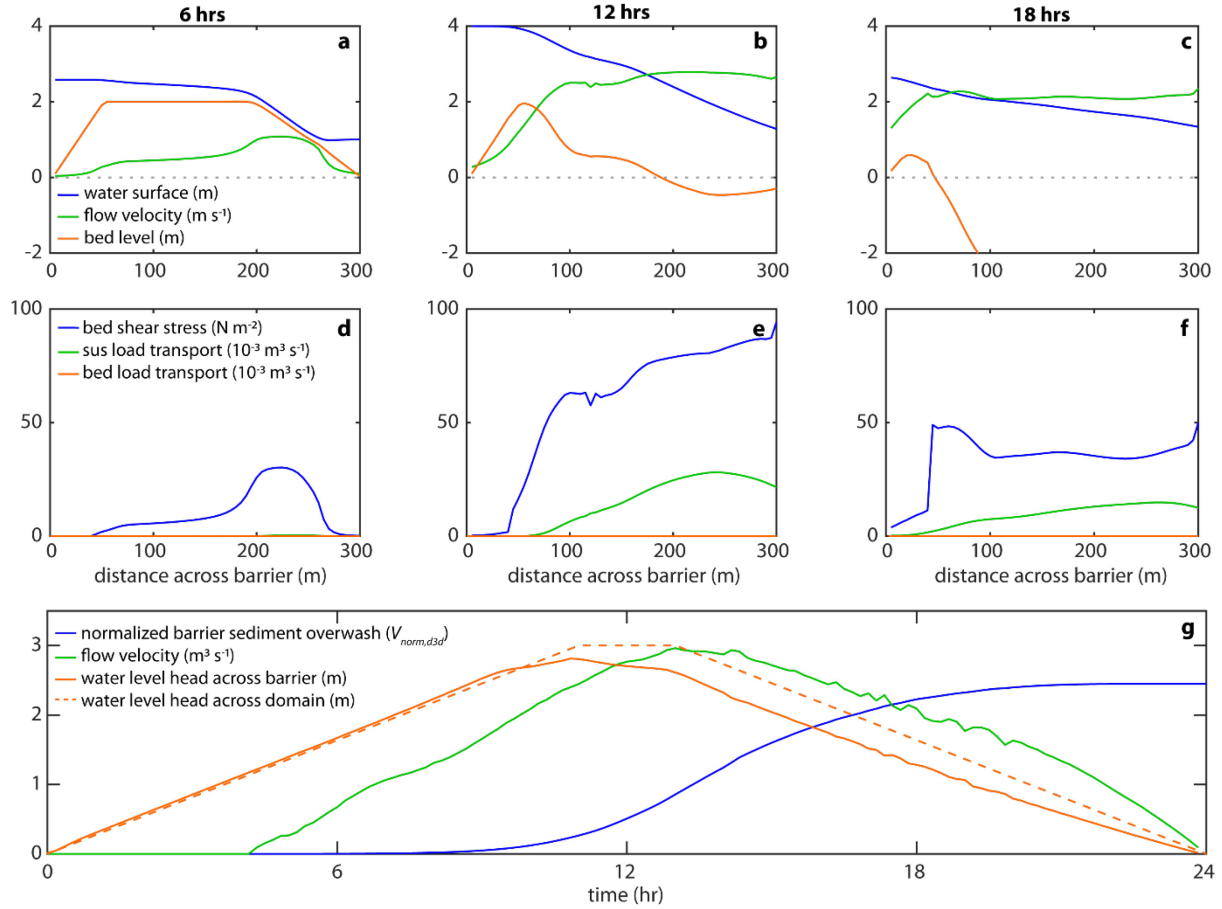
332 the first 12 hours of the storm.

Figure 5. (**a**, **b**, **c**) Snapshots of water levels, flow velocities, and bed erosion across a dune gap at 6, 12, and 18 hours of a 24 hour storm surge event. (**d**, **e**, **f**) Bed shear stress and sediment transport through the dune gap. (**g**) Time-series of water level differences and velocities across the barrier, resulting in a high normalized barrier overwashing flux ($V_{norm,obs}$) of ~2.4. This indicates that the barrier is likely to be breached.

5.2   Breaching vs. washover deposits

We contrast the event from section 5.1 that resulted in a breach with another simulation where a washover was deposited (Fig. 6). The washover formed following a 2.2-m storm surge. Water discharge and suspended sediment transport across the dune gap develop in tandem, and erosion primarily acts on the back of the dune gap. A small, 1700 m^3 washover fan develops (Fig. 6, top panel).

We find similarities between the initial development of the barrier breach and washover deposit: a small washover fan also appears in response to the breach, although it is more disperse

16

347   (Fig. 6, at 12h). This makes intuitive sense, sediment eroded from a breach must deposit

348   somewhere. These "breach" deposits are not commonly found. Under natural conditions these

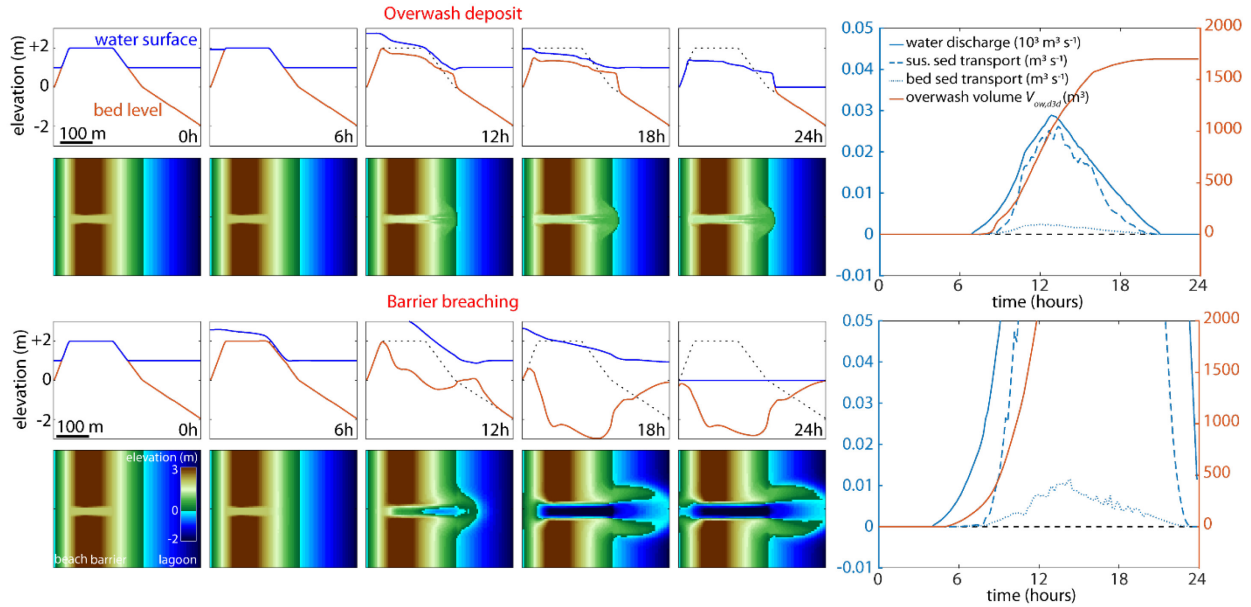349   deposits could be transported oceanward during a return flow through the breach (Basco & Shin,

350   1999).

351

352   **Figure 6.** A 2.2 m and 3 m peak storm surge resulted in the development of a washover (top

353   panel) and barrier breach (bottom panel), respectively. Corresponding figures show the

354   morphologic evolution during the storm and timeseries of overwashing water and sediment.

355   Dotted lines indicate pre-storm barrier profile.

356   *5.3   Predicting breach and washover events*

357   In 139 simulations we varied storm characteristics and barrier morphologies (Table 1) to

358   better understand controls on washover and barrier breach development. Across all simulations,

359   we find that the overwashing sediment transport fluxes ($V_{ow,d3d}$) range from 0 (no overwash) to

360   $3.3 \cdot 10^5$ m^3. Barrier subaerial volumes (V_{bar}), in comparison, range from $2.6 \cdot 10^3$ to $5.2 \cdot 10^4$ m^3.

361   Normalized overwashing fluxes ($V_{norm,d3d}$) vary between 0 and 12.7.

362   In 26 simulations the storms resulted in barrier breaches, defined as an open water

363   connection between the ocean and the bay at mean sea level (Fig. 7a). For the large majority of

364   the simulations, the threshold $V_{norm,d3d} = 1$ separates storm conditions that lead to barrier

365   washover deposition and barrier breaching. For one simulation we find that a breach occurred

17

366   despite the normalized overwashing flux $V_{norm,d3d} < 1$ because erosion across the dune gap was

367   not uniform and resulted in a narrow breach. Similarly, for three simulations, the barrier

368   remained intact and $V_{norm,d3d} > 1$.

369   Comparing the Delft3D storm impacts ($V_{norm,d3d}$) against predicted storm impact ($V_{norm,t}$

370   eq. 5) we find that it explains a significant amount of the variation between the model runs (Fig.

371   7b). Washover volumes increase for increasing predicted overwashing flux ($V_{ow,t}$). The majority

372   of storms result in barrier breaches for $V_{norm,t} > 1$, and 80% of all simulations result in barrier

373   breaches if $V_{norm,t} > 4$ (Fig. 7c).

374   Our predictor scales linearly with sediment transport and misses some non-linear effects.

375   Predicted storm impacts $V_{norm,t}$ vary across 3 orders of magnitude whereas our simulations

376   ($V_{norm,obs}$) vary across 5 orders of magnitude. One non-linear effect results from the influence of

377   the dune gap width (w_g) on overwash fluxes. It is apparent in the vertical stacks of experimental

378   results in Fig. 7b, which arise because the dune gap width does not affect $V_{norm,t}$ (eq. 5). We find

379   that, in contrast to Wesselman (2019), larger gap widths lead to greater overwashing flow

380   velocities: the decrease in flow friction for larger gaps outweighs the effects of flow constriction.

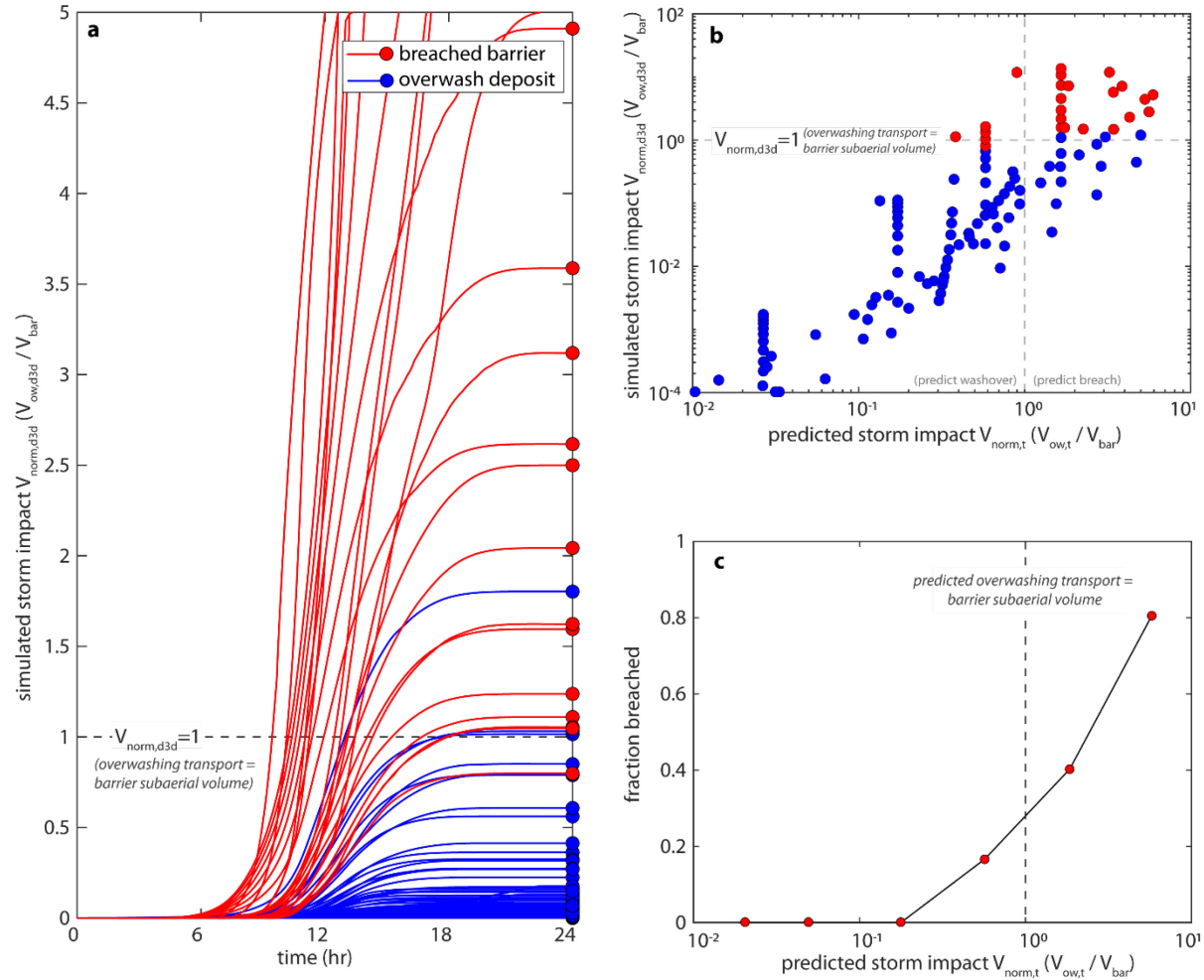381   A linear increase in gap width results in a supralinear increase in overwashing sediment fluxes.

Figure 7. (**a**) Time evolution of overwashing sediment transport for varying storm and barrier characteristics, normalized by the subaerial barrier volume. Red lines indicate simulations where storms led to barrier breaching. (**b**) Simulated overwashing sediment flux ($V_{norm,d3d}$) compared to the predicted sediment flux ($V_{norm,t}$). (**c**) Fraction of simulations resulting in breached barriers as a function of predicted storm impact ($V_{norm,t}$).

5.4   Comparison of simulations against observations from Hurricane Sandy

How do the observations from Hurricane Sandy fit within the variability of the Delft3D simulations? First, we find overwash volumes from Hurricane Sandy occupy a narrow range compared to our simulated volumes from Delft3D (Fig. 8). This range in observed volumes is also much narrower than what we predict using our conceptual model (eq. 4 and 5), and indicates a (relatively) low sensitivity to storm characteristics and barrier morphology. Earlier studies have also noted this and resorted to using a sediment transport limiter (e.g., McCall et al., 2010).

19

395   A closer inspection into the Sandy observations shows a large difference between natural

396   and developed coasts. We find that the overwash volumes for developed coastlines are smaller

397   than those along undeveloped coasts (mean of 200 m³ and 370 m³, respectively). Although there

398   is a risk of selection or observation bias (e.g., Lazarus & Goldstein, 2019), other studies have

399   also found a large effect of development on overwash dynamics. Structures block flow and

400   pavement limits erosion (Rogers et al., 2015).

401   The magnitudes and trends of Hurricane Sandy overwashes and breaches that formed on

402   natural (undeveloped) coasts are similar to our Delft3D observations (Fig. 8). This general

403   agreement highlights the importance of the parameters in our predictor (barrier width, barrier

404   height, and storm surge height) on barrier morphologic response. Of the 4 natural coast

405   overwashing flows with a predicted storm impact $V_{norm,t} > 1$, 3 resulted in breaches. Of the

406   overwashing flows with a predicted storm impact $V_{norm,t} < 1$, washover fans appeared in 86% of

407   the cases. However, caution remains because there is significant scatter around these trends.

408   Detailed, site-specific simulations (e.g., van Ormondt et al., 2020) are likely to be much more
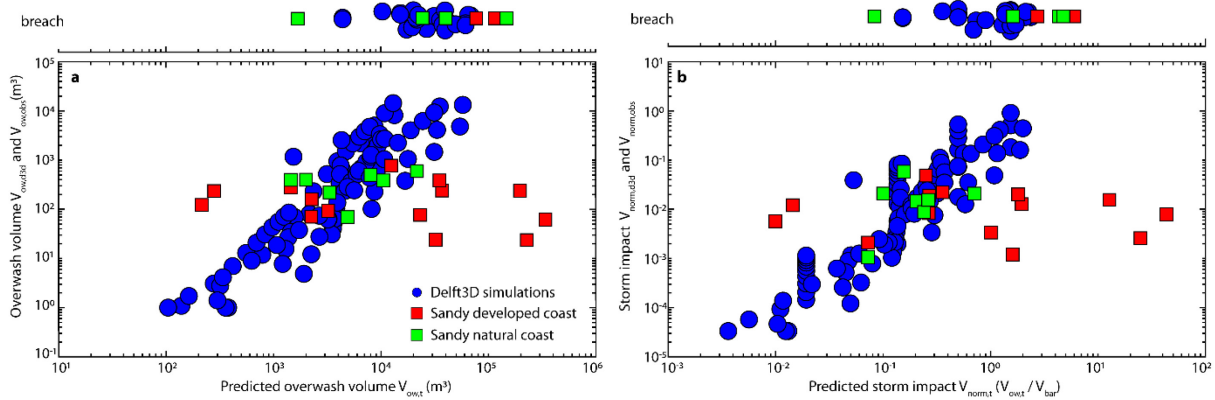
409   accurate for individual cases.

410

Figure 8. (**a**) Predicted vs. observed overwashing volume and (**b**) storm impacts for Delft3D

simulations and Hurricane Sandy observations. Breaches (which in the case of Sandy

observations have no observed overwash volume) are plotted separately. The observed

variability in storm impacts on developed coasts (red squares) is not captured by our predictor.

415   In contrast to our observations for natural coasts, we do not observe any trends in the

416   breaches and overwash fans that formed along developed coasts. Some of the developed coast

417 breaches had a very low breaching probability ($V_{norm.t} \approx 0.4$), whereas observed overwash fans

418 along developed coastlines formed despite a predicted breach ($V_{norm,t} = 43$). This would imply

419 that variables that are not included in our predictor (to the correct extent), such as the erodibility

420 of pavement or surface heterogeneity that funnels or disperses overwashing flows, dominates the

421 response to storms for developed coasts.

422 **6   Discussion**

423   In this study we developed and tested an analytical theory for the development of

424 washover fans and barrier breaches. In general, the simulations and predictors are simplified

425 compared to natural dynamics of overwashing flows, which allowed us to formulate an analytic

426 formulation that is integrated over the duration of the storm. Here we will discuss potential uses

427 from the resulting formulation and the observed (mis) matches with data.

428 *6.1   Implications for paleo environmental reconstructions*

429   Washover fan deposits are often used to reconstruct storms and climatic conditions

430 (Woodruff et al., 2008; Shaw et al., 2015; Mulhern et al., 2019). Fan size and internal

431 stratigraphy can record storm tracks, but bracketing storm intensity remain challenging. Our

432 storm impact predictor (eq. 5) can be used as an inverse model to reconstruct paleo-storms where

433 detailed models might not be appropriate because accurate boundary conditions and initial

434 conditions are difficult to obtain. For example, our predictor could indicate a minimum storm

435 intensity that would result in the formation of a washover fan with a certain observed volume or

436 thickness. The presence of a preserved washover fan also indicates that the storm did not breach

437 the barrier.

438 *6.2   Implications for morphodynamic barrier island models*

439   The landward sediment transport of barrier overwashing flows is important for the long-

440 term survival of barrier islands facing sea-level rise (Storms, 2003; Nienhuis & Lorenzo-Trueba,

441 2019a). Models have been developed to investigate overwashing fluxes and long-term barrier

442 dynamics (Ashton & Lorenzo-Trueba, 2018; Nienhuis & Lorenzo-Trueba, 2019b), but scale-

443 discrepancies still exist between our understanding of individual storms and barrier island

444 transgression.

445   Current state-of-the-art barrier island models (Lorenzo-Trueba & Ashton, 2014) are
446   reliant on empirical concepts that estimate washover deposition based on a distance function
447   away from the current shoreline (Storms et al., 2002) or a certain critical barrier width
448   (Leatherman, 1979; Jiménez & Sánchez-Arcilla, 2004; Rosati & Stone, 2007). This latter
449   concept suggests that washover deposition into the lagoon only occurs if barrier width is below a
450   certain (critical) width. The overwash flux is then estimated based on how much the barrier
451   width deviates from the critical width, and sometimes is also limited to be below a certain
452   maximum flux (Lorenzo-Trueba & Ashton, 2014). The shape and limits of these overwash
453   function are important parameters that affect barrier model persistence under sea-level rise.

454   Our predictor could help quantify expected overwash fluxes for different storm climates.
455   We find a strong relation between barrier width and overwashing volume (eq. 4), which, as
456   suggested by the critical width concept, supports a negative feedback that would help barriers
457   retain a certain width (Fig. 9a). Delft3D simulations do not point to a maximum overwash flux,
458   although a possible maximum (storm-integrated) flux could be the subaerial barrier volume. Any
459   greater overwash flux would breach the barrier (Fig. 9b), and potentially result in seaward
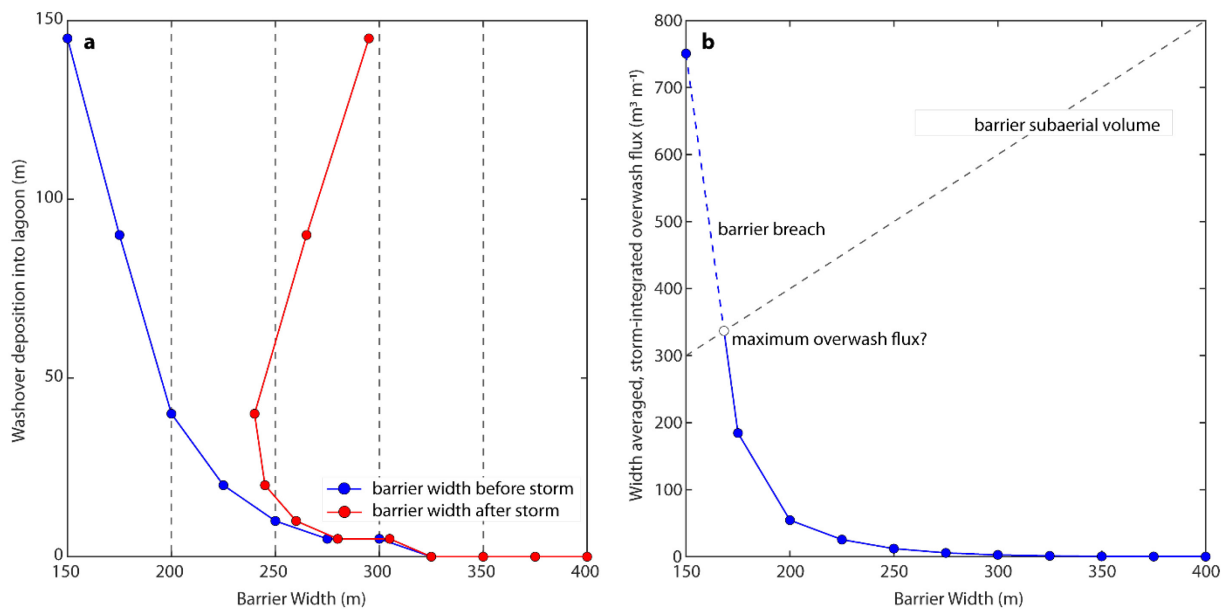460   sediment transport through a return current (e.g., Basco & Shin, 1999).

461

462 **Figure 9:** (**a**) Influence of barrier width on barrier washover distance and post-storm width for a
463 selection of the Delft3D model simulations. Note that the red line is simply the sum of the
464 original width (x-axis) and the added washover width (y-axis). (**b**) Influence of barrier width on
465 the alongshore- averaged overwash flux. A alongshore-averaged flux that exceeds the subaerial
466 barrier volume (V_{bar}) results in a breach. This provides some indication that the maximum
467 preserved overwash flux could be equal to the barrier volume.

468 **7   Conclusions**

469   In this study we proposed that barrier islands breach when the cumulative sediment flux
470 of an overwashing flow exceeds the barrier subaerial volume (eq. 5). Washover volumes increase
471 as overwashing flows approach the washover-to-breaching threshold: the largest washover fans
472 likely appear when storms were very close to creating a breach. Tests against idealized Delft3D
473 simulations show good agreement, although a calibration factor was necessary. We find
474 reasonable agreement with observations of natural coastline response to Hurricane Sandy, and no
475 agreement for overwashing across developed coasts.

476   Our study demonstrates the sensitivity of barrier width and storm surge height on barrier
477 breaching and washover deposition. Increasing storm surge height raises the water depth and
478 water surface slope of overwashing flows. Increasing barrier width reduces the water surface
479 slope and increases the barrier subaerial volume. Barrier height and barrier vegetation reduce the
480 likelihood of barrier breaching, whereas storm duration will increase it. Our predictor could be
481 useful for estimates of barrier landward sediment fluxes in the face of sea-level rise, as well as
482 paleo-environmental studies of (extra) tropical cyclone dynamics.

490   **8   References**

491   Ashton, A. D., & Lorenzo-Trueba, J. (2018). Morphodynamics of Barrier Response to Sea-Level

492   Rise. In *Barrier Dynamics and Response to Changing Climate* (pp. 277–304). Cham:

493   Springer International Publishing. https://doi.org/10.1007/978-3-319-68086-6_9

494   Baptist, M. J., Babovic, V., Uthurburu, J. R., Keijzer, M., Uittenbogaard, R. E., Mynett, A., …

495   Hoffmann, M. R. (2009). On inducing equations for vegetation resistance. *Journal of*

496   *Hydraulic Research*, *45*(4), 435–450. https://doi.org/10.1080/00221686.2007.9521778

497   Basco, D. R., & Shin, C. S. (1999). A one-dimensional numerical model for storm-breaching of

498   barrier islands. *Journal of Coastal Research*, *15*(1), 241–260.

499   Biel, R. G., Hacker, S. D., Ruggiero, P., Cohn, N., & Seabloom, E. W. (2017). Coastal protection

500   and conservation on sandy beaches and dunes: context-dependent tradeoffs in ecosystem

501   service supply. *Ecosphere*, *8*(4). https://doi.org/10.1002/ecs2.1791

502   Birchler, J. J., Dalyander, P. S., Stockdon, H. F., & Doran, K. S. (2015). *National Assessment of*

503   *Nor'easter-Induced Coastal Erosion Hazards: Mid- and Northeast Atlantic Coast*. Reston,

504   VA. https://doi.org/10.3133/ofr20151154

505   Booij, N., Ris, R. C., & Holthuijsen, L. H. (1999). A third-generation wave model for coastal

506   regions 1. Model description and validation. *Journal of Geophysical Research*, *104*(C4),

507   7649. https://doi.org/10.1029/98JC02622

508   Carruthers, E. A., Lane, D. P., Evans, R. L., Donnelly, J. P., & Ashton, A. D. (2013).

509   Quantifying overwash flux in barrier systems: An example from Martha's Vineyard,

510   Massachusetts, USA. *Marine Geology*, *343*, 15–28.

511   https://doi.org/10.1016/j.margeo.2013.05.013

512   Deltares. (2014). *User Manual Delft3D* (No. 4.00). Delft, The Netherlands: Deltares. Retrieved

513   from www.delftsoftware.com

514   Dietrich, J. C., Tanaka, S., Westerink, J. J., Dawson, C. N., Luettich, R. A., Zijlema, M., …

515   Westerink, H. J. (2012). Performance of the Unstructured-Mesh, SWAN+ADCIRC Model

516   in Computing Hurricane Waves and Surge. *Journal of Scientific Computing*, *52*(2), 468–

497. https://doi.org/10.1007/s10915-011-9555-6

Van Dongeren, A., Bolle, A., Vousdoukas, M. I., Plomaritis, T., Eftimova, P., Williams, J., …
Roelvink, D. (2009). Micore: dune erosion and overwash model validation with data from
nine European field sites. In M. Mizuguchi & S. Sato (Eds.), *Proceedings of Coastal
Dynamics 2009* (pp. 1–15). Tokyo, Japan: World Scientific.
https://doi.org/10.1142/9789814282475_0084

Donnelly, C., Kraus, N. C., & Larson, M. (2006). State of Knowledge on Measurement and
Modeling of Coastal Overwash. *Journal of Coastal Research*, *22*(4), 965–991.
https://doi.org/10.2112/04-0431.1

Elsayed, S., & Oumeraci, H. (2016). Combined Modelling of Coastal Barrier Breaching and
Induced Flood Propagation Using XBeach. *Hydrology*, *3*(4), 32.
https://doi.org/10.3390/hydrology3040032

Engelstad, A., Ruessink, B. G., Hoekstra, P., & Vegt, M. (2018). Sand Suspension and Transport
During Inundation of a Dutch Barrier Island. *Journal of Geophysical Research: Earth
Surface*, *123*, 2018JF004736. https://doi.org/10.1029/2018JF004736

Engelund, F., & Hansen, E. (1967). *A monograph on sediment transport in alluvial streams*.
Copenhagen, Denmark: Teknisk Forlag.

Fisher, J. S., & Stauble, D. K. (1977). Impact of Hurricane Belle on Assateague Island washover.
Geology, *5*(12), 765. https://doi.org/10.1130/0091-7613(1977)5<765:IOHBOA>2.0.CO;2

Goff, J. A., Swartz, J. M., Gulick, S. P. S., Dawson, C. N., & de Alegria-Arzaburu, A. R. (2019).
An outflow event on the left side of Hurricane Harvey: Erosion of barrier sand and seaward
transport through Aransas Pass, Texas. *Geomorphology*, *334*, 44–57.
https://doi.org/10.1016/j.geomorph.2019.02.038

Hayes, M. O. (1979). Barrier island morphology as a function of tidal and wave regime. In S. P.
Leatherman (Ed.), *Barrier Islands* (pp. 1–27). New York, USA: Academic Press.

Houser, C., Hapke, C., & Hamilton, S. (2008). Controls on coastal dune morphology, shoreline
erosion and barrier island response to extreme storms. *Geomorphology*, *100*(3–4), 223–240.

544   https://doi.org/10.1016/j.geomorph.2007.12.007

545   Hudock, J. W., Flaig, P. P., & Wood, L. J. (2014). Washover fans: A modern geomorphologic

546   analysis and proposed classification scheme to improve reservoir models. *Journal of*

547   *Sedimentary Research*, *84*(10), 854–865. https://doi.org/10.2110/jsr.2014.64

548   Jiménez, J. A., & Sánchez-Arcilla, A. (2004). A long-term (decadal scale) evolution model for

549   microtidal barrier systems. *Coastal Engineering*, *51*(8–9), 749–764.

550   https://doi.org/10.1016/j.coastaleng.2004.07.007

551   Kobayashi, N. (2010). Wave Overtopping of Levees and Overwash of Dunes. *Journal of Coastal*

552   *Research*, *2010*(265), 888–900. https://doi.org/10.2112/JCOASTRES-D-09-00034.1

553   Kraus, N. C., & Hayashi, K. (2005). Numerical morphologic model of barrier island breaching.

554   In *Proceedings of the Coastal Engineering Conference*.

555   https://doi.org/10.1142/9789812701916-0170

556   Kraus, N. C., Militello, A., & Todoroff, G. (2002). Barrier Beaching Processes and Barrier Spit

557   Breach, Stone Lagoon, California. *Shore and Beach*, *70*(4), 21–28.

558   Lazarus, E. D. (2016). Scaling laws for coastal overwash morphology. *Geophysical Research*

559   *Letters*, *43*(23), 12,113-12,119. https://doi.org/10.1002/2016GL071213

560   Lazarus, E. D., & Armstrong, S. (2015). Self-organized pattern formation in coastal barrier

561   washover deposits. *Geology*, *43*(4), 363–366. https://doi.org/10.1130/G36329.1

562   Lazarus, E. D., & Goldstein, E. B. (2019). Is There a Bulldozer in your Model? *Journal of*

563   *Geophysical Research: Earth Surface*, *124*(3), 696–699.

564   https://doi.org/10.1029/2018JF004957

565   Leatherman, S. P. (1979). Migration of Assateague Island, Maryland, by inlet and overwash

566   processes. *Geology*, *7*(2), 104–107. https://doi.org/10.1130/0091-

567   7613(1979)7<104:MOAIMB>2.0.CO;2

568   Lorenzo-Trueba, J., & Ashton, A. D. (2014). Rollover, drowning, and discontinuous retreat:

569   Distinct modes of barrier response to sea-level rise arising from a simple morphodynamic

570   model. *Journal of Geophysical Research: Earth Surface*, *119*(4), 779–801.

571   https://doi.org/10.1002/2013JF002941

572   Luettich, R. A., Westerink, J. J., & Scheffner, N. W. (1992). ADCIRC: An Advanced Three-

573   Dimensional Circulation Model for Shelves Coasts and Estuaries, Report 1: Theory and

574   Methodology of ADCIRC-2DDI and ADCIRC-3DL, Dredging Research Program

575   Technical Report DRP-92-6. *Dredging Research Program Technical Report DRP-92-6,*

576   *U.S. Army Engineers Waterways Experiment Station, Vicksburg, MS,*.

577   Mallinson, D. J., Smith, C. W., Culver, S. J., Riggs, S. R., & Ames, D. (2010). Geological

578   characteristics and spatial distribution of paleo-inlet channels beneath the outer banks

579   barrier islands, North Carolina, USA. *Estuarine, Coastal and Shelf Science*, *88*(2), 175–189.

580   https://doi.org/10.1016/j.ecss.2010.03.024

581   McCall, R. T., Van Thiel de Vries, J. S. M., Plant, N. G., Van Dongeren, A. R., Roelvink, J. A.,

582   Thompson, D. M., & Reniers, A. J. H. M. (2010). Two-dimensional time dependent

583   hurricane overwash and erosion modeling at Santa Rosa Island. *Coastal Engineering*, *57*(7),

584   668–683. https://doi.org/10.1016/j.coastaleng.2010.02.006

585   Morgan, K. L. M. (2009). *Coastal change during Hurricane Ivan 2004: U.S. Geological Survey*

586   *Fact Sheet 2009-3026*. Reston, VA.

587   Morton, R. A., Sallenger Jr., A. H., & Sallenger, A. H. (2003). Morphological Impacts of

588   Extreme Storms on Sandy Beaches and Barriers. *Journal of Coastal Research*, *19*(3), 560–

589   573. https://doi.org/10.2307/4299198

590   Mulhern, J. S., Johnson, C. L., & Martin, J. M. (2019). Modern to Ancient Barrier Island

591   Dimensional Comparisons: Implications for Analog Selection and Paleomorphodynamics.

592   *Frontiers in Earth Science*, *7*. https://doi.org/10.3389/feart.2019.00109

593   Nguyen, X.-T., Donnelly, C., Tanaka, H., & Larson, M. (2009). A new empirical formula for

594   coastal washover sediment volume. In *Coastal Engineering 2008* (pp. 1736–1748). World

595   Scientific Publishing Company. https://doi.org/10.1142/9789814277426_0144

596   Nienhuis, J. H., Törnqvist, T. E., & Esposito, C. R. (2018). Crevasse Splays Versus Avulsions: A

597   Recipe for Land Building With Levee Breaches. *Geophysical Research Letters*, *45*(9),

598   4058–4067. https://doi.org/10.1029/2018GL077933

599   Nienhuis, J. H., & Lorenzo-Trueba, J. (2019a). Can Barrier Islands Survive Sea-Level Rise?

600   Quantifying the Relative Role of Tidal Inlets and Overwash Deposition. *Geophysical*

601   *Research Letters*, *46*(24), 14613–14621. https://doi.org/10.1029/2019GL085524

602   Nienhuis, J. H., & Lorenzo-Trueba, J. (2019b). Simulating barrier island response to sea level

603   rise with the barrier island and inlet environment (BRIE) model v1.0. *Geoscientific Model*

604   *Development*, *12*(9), 4013–4030. https://doi.org/10.5194/gmd-12-4013-2019

605   van Ormondt, M., Nelson, T. R., Hapke, C. J., & Roelvink, D. (2020). Morphodynamic

606   modelling of the wilderness breach, Fire Island, New York. Part I: Model set-up and

607   validation. *Coastal Engineering*, *157*, 103621.

608   https://doi.org/10.1016/j.coastaleng.2019.103621

609   Passeri, D. L., Dalyander, P. S., Long, J. W., Mickey, R. C., Jenkins, R. L., Thompson, D. M., …

610   Gonzalez, V. M. (2020). The Roles of Storminess and Sea Level Rise in Decadal Barrier

611   Island Evolution. *Geophysical Research Letters*, *47*(18).

612   https://doi.org/10.1029/2020GL089370

613   Passeri, D. L., Long, J. W., Plant, N. G., Bilskie, M. V., & Hagen, S. C. (2018). The influence of

614   bed friction variability due to land cover on storm-driven barrier island morphodynamics.

615   *Coastal Engineering*, *132*, 82–94. https://doi.org/10.1016/j.coastaleng.2017.11.005

616   Pierce, J. W. (1970). Tidal Inlets and Washover Fans. *The Journal of Geology*, *78*(2), 230–234.

617   Plomaritis, T. A., Ferreira, Ó., & Costas, S. (2018). Regional assessment of storm related

618   overwash and breaching hazards on coastal barriers. *Coastal Engineering*, *134*, 124–133.

619   https://doi.org/10.1016/j.coastaleng.2017.09.003

620   van Rijn, L. C. (2007). Unified View of Sediment Transport by Currents and Waves. I: Initiation

621   of Motion, Bed Roughness, and Bed-Load Transport. *Journal of Hydraulic Engineering*,

622   *133*(6), 649–667. https://doi.org/10.1061/(ASCE)0733-9429(2007)133:6(649)

623   Roelvink, D., Reniers, A., van Dongeren, A., van Thiel de Vries, J., McCall, R., & Lescinski, J.

(2009). Modelling storm impacts on beaches, dunes and barrier islands. *Coastal Engineering, 56*(11–12), 1133–1152. https://doi.org/10.1016/j.coastaleng.2009.08.006

Rogers, L. J., Moore, L. J., Goldstein, E. B., Hein, C. J., Lorenzo-Trueba, J., & Ashton, A. D. (2015). Anthropogenic controls on overwash deposition: Evidence and consequences. *Journal of Geophysical Research: Earth Surface, 120*(12), 2609–2624. https://doi.org/10.1002/2015JF003634

Rosati, J. D., & Stone, G. W. (2007). Critical Width of Barrier Islands and Implications for Engineering Design. In N. C. Kraus & J. D. Rosati (Eds.), *Coastal Sediments '07* (pp. 1988–2001). Reston, VA: American Society of Civil Engineers. https://doi.org/10.1061/40926(239)156

Sallenger, A. H. (2000). Storm impact scale for barrier islands. *Journal of Coastal Research, 16*(3), 890–895.

Sánchez-Arcilla, A., & Jiménez, J. A. (1994). Breaching in a wave-dominated barrier spit: The trabucador bar (north-eastern spanish coast). *Earth Surface Processes and Landforms, 19*(6), 483–498. https://doi.org/10.1002/esp.3290190602

Sedrati, M., Ciavola, P., & Armaroli, C. (2011). Morphodynamic evolution of a microtidal barrier, the role of overwash: Bevano , Northern Adriatic Sea. *Journal of Coastal Research, SI 64*(ICS2011), 696–700.

Shaw, J., You, Y., Mohrig, D., & Kocurek, G. (2015). Tracking hurricane-generated storm surge with washover fan stratigraphy. *Geology, 43*(2), 127–130. https://doi.org/10.1130/G36460.1

Shin, C. S. (1996). *A One-Dimensional Model for Storm Breaching of Barrier Islands*. Old Dominion University. https://doi.org/10.25777/3cjy-xw31

Smallegan, S. M., Irish, J. L., Van Dongeren, A. R., & Den Bieman, J. P. (2016). Morphological response of a sandy barrier island with a buried seawall during Hurricane Sandy. *Coastal Engineering, 110*, 102–110. https://doi.org/10.1016/j.coastaleng.2016.01.005

Sopkin, K. L., Stockdon, H. F., Doran, B. K. S., Plant, N. G., Morgan, K. L. M., Guy, K. K., & Smith, K. E. L. (2014). *Hurricane Sandy: observations and analysis of coastal change. U.S.*

651   *Geological Survey Open-File Report 2014-1088*.

652 Storms, J. E. A. (2003). Event-based stratigraphic simulation of wave-dominated shallow-marine
653   environments. *Marine Geology*, *199*(1–2), 83–100. https://doi.org/10.1016/S0025-
654   3227(03)00144-0

655 Storms, J. E. A., Weltje, G. J., van Dijke, J. J., Geel, C. R., & Kroonenberg, S. B. (2002).
656   Process-Response Modeling of Wave-Dominated Coastal Systems: Simulating Evolution
657   and Stratigraphy on Geological Timescales. *Journal of Sedimentary Research*, *72*(2), 226–
658   239. https://doi.org/10.1306/052501720226

659 Suter, J. R., Nummedal, D., Maynard, A. K., & Kemp, P. (1982). A Process-Response Model for
660   Hurricane Washovers. In *Coastal Engineering 1982* (pp. 1459–1478). New York, NY:
661   American Society of Civil Engineers. https://doi.org/10.1061/9780872623736.089

662 Tuan, T. Q., Stive, M. J. F., Verhagen, H. J., & Visser, P. J. (2008). Process-based modeling of
663   the overflow-induced growth of erosional channels. *Coastal Engineering*, *55*(6), 468–483.
664   https://doi.org/10.1016/j.coastaleng.2008.01.002

665 De Vet, P. L. M., McCall, R. T., Den Bieman, J. P., Stive, M. J. F., & van Ormondt, M. (2015).
666   Modelling dune erosion, overwash, and breaching at Fire Island (NY) during Hurricane
667   Sandy. In P. Wang, J. D. Rosati, & J. Cheng (Eds.), *The Proceedings of the Coastal*
668   *Sediments 2015* (p. 5). San Diego, USA: World Scientific Pub Co Inc.
669   https://doi.org/10.1142/9789814689977_0006

670 Visser, P. J. (2001). A Model for Breach Erosion in Sand-Dikes. In *Coastal Engineering* (Vol.
671   276, pp. 3829–3842). Reston, VA: American Society of Civil Engineers.
672   https://doi.org/10.1061/40549(276)299

673 Wesselman, D., de Winter, R., Engelstad, A., McCall, R., van Dongeren, A., Hoekstra, P., …
674   van der Vegt, M. (2018). The effect of tides and storms on the sediment transport across a
675   Dutch barrier island. *Earth Surface Processes and Landforms*, *43*(3), 579–592.
676   https://doi.org/10.1002/esp.4235

677 Wesselman, D., de Winter, R., Oost, A., Hoekstra, P., & van der Vegt, M. (2019). The effect of

678   washover geometry on sediment transport during inundation events. *Geomorphology*, *327*,

679   28–47. https://doi.org/10.1016/j.geomorph.2018.10.014

680   Williams, P. J. (1978). *Laboratory development of a predictive relationship for washover volume*

681   *on barrier island coastlines*. Department of Civil Engineering, University of Delaware, p.

682   154.

683   de Winter, R. C., Gongriep, F., & Ruessink, B. G. (2015). Observations and modeling of

684   alongshore variability in dune erosion at Egmond aan Zee, the Netherlands. *Coastal*

685   *Engineering*, *99*, 167–175. https://doi.org/10.1016/j.coastaleng.2015.02.005

686   Woodruff, J. D., Donnelly, J. P., Mohrig, D., & Geyer, W. R. (2008). Reconstructing relative

687   flooding intensities responsible for hurricane-induced deposits from Laguna Playa Grande,

688   Vieques, Puerto Rico. *Geology*, *36*(5), 391. https://doi.org/10.1130/G24731A.1

689